Int. J. Heat Mass Transfer. Vol. 34, No. 8, pp. 2029–2037, 1991
Printed in Great Britain

0017–9310/91 $3.00+0.00

Analysis of the one-dimensional transient compressible vapor flow in heat pipes

JONG HOON JANG† and AMIR FAGHRI
Department of Mechanical and Materials Engineering, Wright State University, Dayton, OH 45435, U.S.A.

and

WON SOON CHANG
Wright Research and Development Center, Wright-Patterson AFB, OH 45433-6563, U.S.A.

(*Received* 4 *May* 1990 *and in final form* 21 *September* 1990)

Abstract—The transient compressible one-dimensional vapor flow dynamics in a heat pipe is modeled. The numerical results are obtained by using the implicit non-iterative Beam-Warming finite difference method. The model is tested for simulated heat pipe vapor flow and actual vapor flow in cylindrical heat pipes. A good comparison of the present transient results for the simulated heat pipe vapor flow with the previous results of a two-dimensional numerical model is achieved and the steady state results are in agreement with the existing experimental data. The transient behavior of the vapor flow under subsonic, sonic, and supersonic speeds as well as high mass flow rates are successfully predicted.

1. INTRODUCTION

IN A HEAT pipe, the change of phase of the working fluid in the closed system is used instead of a large temperature gradient to transport a large amount of energy. The attention of many scientists has focused on this unique phenomenon since the concept was introduced. The vapor from the evaporator carries energy to the condenser, so the vapor flow in the core region of the heat pipe plays an important role in transferring energy from source to sink.

Many researchers have studied the steady one-dimensional compressible vapor flow [1–4] and the steady two-dimensional vapor flow in heat pipes [3, 5–9]. The common cross sections of the vapor space are circular, rectangular [4, 7, 9] and annular [3, 8] and are chosen based on the particular application. The heat flux distributions on the surface of the evaporator and condenser are uniform around the circumference except for those presented in refs. [4, 10]. Recently, the transient two-dimensional compressible simulated vapor flow in heat pipes [11, 12] was solved numerically, and the experimental data for the steady state simulated heat pipe vapor flow was obtained [11]. However, the vapor flow was not actual vapor flow in a heat pipe and the numerical and experimental data were presented only in terms of the pressure. The transient two-dimensional compressible vapor flow in a heat pipe with a circular cross section was studied numerically [13]. The numerical results for both simulated compressible vapor flow with high Mach numbers and the vapor flow of a high temperature heat pipe were compared with the experimental data in the literature. The transient responses of heat pipes to a pulsed heat input were also investigated.

During the start-up of high temperature heat pipes, the extremely small density of the vapor causes the vapor flow to attain sonic and supersonic velocities for a relatively small heat input [14]. Thus, the correct description of the transient vapor flow is essential to predict the successful start-up and to estimate the overall performance of the entire heat pipe. The governing equations for the vapor flow as well as those for the wall and wick regions should be solved simultaneously. Also, the development of the one-dimensional transient model for the vapor flow has been suggested due to the large amount of computer time required for the two-dimensional model [11, 12]. For this purpose, a simple and efficient mathematical model is desired for each region. All previous one-dimensional models for vapor flow are for the steady state condition.

This paper describes the mathematical model and the numerical method of solution for the transient compressible one-dimensional vapor flow in heat pipes. A comparison of the numerical results with the simulated transient two-dimensional numerical results and experimental data for the steady state given by ref. [11] is also presented. In addition, the numerical results from the present model for the actual vapor flow in the cylindrical high temperature heat pipe are compared with the experimental data obtained at the steady state [15].

† Current address: Sverdrup Technology Inc., NASA Lewis Research Center, Cleveland, OH 44135, U.S.A.

NOMENCLATURE

C_p	specific heat at constant pressure [J kg^{-1} K^{-1}]
C_v	specific heat at constant volume [J kg^{-1} K^{-1}]
D_v	diameter of the vapor space [m]
E_t	total energy of the vapor per unit volume, $\rho(C_vT+1/2\,U^2)$
f	friction coefficient at the wall, $\tau_0/\rho U^2$
f_e	friction coefficient at the exit of the evaporator
f_t	friction coefficient for the fully developed turbulent flow
h	enthalpy [J kg^{-1}]
H_{fg}	latent heat of vaporization [J kg^{-1}]
K	thermal conductivity of the vapor [W m^{-1} K^{-1}]
L	length of the heat pipe [m]
L_a	length of the adiabatic section [m]
L_c	length of the condenser [m]
L_e	length of the evaporator [m]
M	Mach number, $U/\sqrt{(\gamma RT)}$
n	time step
P	vapor pressure [N m^{-2}]
P_c	reference pressure for the Clausius–Clapeyron equation [N m^{-2}]
P_e	pressure at the evaporator end cap [N m^{-2}]
P_{sk}	sink pressure [N m^{-2}]
P_{so}	source pressure [N m^{-2}]
Q	heat input [W]
q	heat flux [W m^{-2}]
R	gas constant [J kg^{-1} K^{-1}]
Re	axial Reynolds number, $\rho UD_v/\mu$
Re_0	radial Reynolds number at the wall, $\rho V_0D_v/\mu$
t	time [s]
T	vapor temperature [K]
T_c	reference temperature for the Clausius–Clapeyron equation [K]
U	axial velocity [m s^{-1}]
V_0	radial velocity at the wall [m s^{-1}]
x	coordinate in the axial direction
$x_{t,i}$	initial location of the transition region [m]
$\bar{x}$	dimensionless location of the transition region, $(x-x_{t,i})/\Omega$.

Greek symbols

γ	ratio of specific heats, C_p/C_v
δt	time increment [s]
δx	distance between nodes [m]
Γ	fraction of transition to turbulent flow
μ	dynamic viscosity [N s m^{-2}]
ρ	density [kg m^{-3}]
τ	shear stress
Ω	$x_{\Gamma=3/4}-x_{\Gamma=1/4}$.

Subscripts

0	properties of the injected or extracted fluid at the wall
x	derivative with respect to x.

2. MATHEMATICAL MODELING

The one-dimensional transient compressible vapor flow is considered to predict the vapor flow dynamics in the heat pipe. Even though a uniform velocity is used, the friction at the interface is incorporated by using the expressions for the friction coefficients, which are found from the two-dimensional numerical results given by ref. [11]. The vapor is assumed to be a perfect gas. The governing equations for the vapor flow in the heat pipe with negligible body forces are formulated by using the principles of the conservation of mass, momentum, and energy in a control volume of cross-sectional area, $\pi D_v^2/4$, and width, dx.

The governing equations are written in a compact vectorial form as follows:

$$\frac{\partial D}{\partial t}+\frac{\partial E(D)}{\partial x}=\frac{\partial}{\partial x}F(D,D_x)+G \tag{1}$$

where

$$D=\begin{bmatrix}\rho\\ \rho U\\ E_t\end{bmatrix} \tag{2}$$

$$E(D)=\begin{bmatrix}\rho U\\ \rho U^2+P\\ U(E_t+P)\end{bmatrix} \tag{3}$$

$$F(D,D_x)=\begin{bmatrix}0\\ \frac{4}{3}\mu\frac{\partial U}{\partial x}\\ \frac{4}{3}\mu\frac{\partial U}{\partial x}U+K\frac{\partial T}{\partial x}\end{bmatrix} \tag{4}$$

$$G=\begin{bmatrix}\frac{4}{D_v}\rho_0V_0(x)\\ -\frac{2\rho U^2f}{D_v}\\ \left\{\frac{4\rho_0V_0(x)}{D_v}\left(h_0(x)+\frac{V_0^2(x)}{2}\right)\right\}\end{bmatrix} \tag{5}$$

where $V_0(x)$ refers to the velocity at the wall with a positive value for injection and a negative value for suction.

The equation of state is employed to relate the

density, pressure, and temperature in the vapor space as follows:

$$P = \rho RT. \tag{6}$$

For the simulated heat pipe vapor flow, the temperature was evaluated by using the equation of state because a change of phase was not involved. For the actual vapor flow in the cylindrical heat pipe, the Clausius–Clapeyron relationship was used to predict the saturation temperature of the vapor from the pressure as given by

$$T = \frac{1}{\frac{1}{T_c} - \frac{R}{H_{fg}} \ln \frac{P}{P_c}}. \tag{7}$$

The known boundary conditions at the ends of the heat pipe are as follows:

$$U = 0 \quad \text{at } x = 0 \quad \text{and} \quad L \tag{8}$$

$$\frac{\partial T}{\partial x} = 0 \quad \text{at } x = 0 \quad \text{and} \quad L. \tag{9}$$

The conditions for the density and pressure at the ends of the heat pipe are unknown, so physically realistic boundary conditions should be derived. In general, near the ends of the heat pipe the mass flow rate is small, so the axial gradients of the pressure and density are small. In the region adjacent to the exit of the evaporator, the variations of the pressure and density are large. Thus, the boundary conditions for the pressure and density can be assumed as follows:

$$\frac{\partial P}{\partial x} = 0 \quad \text{at } x = 0 \quad \text{and} \quad L \tag{10}$$

$$\frac{\partial \rho}{\partial x} = 0 \quad \text{at } x = 0 \quad \text{and} \quad L. \tag{11}$$

A correlation between the mass flux at the wall and the pressure drop across a porous tube wall based on experimental measurements for the simulated heat pipe vapor flow was given in ref. [11]. The mass flux $(\rho_0 V_0)$ at the wall for the simulated heat pipe vapor flow was evaluated by using this correlation

$$\Delta(P^2) = 3.639 \times 10^9 (\rho_0 V_0)^2 + 1.7015 \times 10^8 (\rho_0 V_0) \tag{12}$$

where $\Delta(P^2)$ is the absolute value of the difference between the square of the uniform source pressure and the square of the vapor pressure in the blowing section. In the suction section, $\Delta(P^2)$ is the absolute value of the difference between the square of the vapor pressure and the square of the uniform sink pressure. A change of phase of the working substance was not involved. The uniform source temperature of 300 K was used for his experiment, but the sink temperature was not specified. To evaluate the terms in braces { } in equation (5), the source temperature is used at the blowing section and the vapor temperature is employed at the suction section.

Since the working fluid changes phase at the vapor–liquid interface in actual heat pipes, the temperature at the interface is the saturation temperature, but the temperature in the vapor space may be quite different from the saturation temperature for high temperature heat pipes. For the one-dimensional model, the properties are area-averaged so that the temperature in the vapor space is not the interface temperature but is also not the saturation temperature. The vapor temperature can be evaluated from the energy equation and the saturation temperature corresponding to the vapor pressure can be obtained from the Clausius–Clapeyron relationship. However, this saturation temperature is not the actual interface temperature either. The correct estimation of the terms in braces { } in equation (5) is uncertain due to using the area-averaged properties. Since a heat pipe is a closed system, the application of the correct values of heat input and output is important. To eliminate this difficulty, terms in braces { } in equation (5) are replaced by using the heat flux applied on the surfaces of the evaporator and the condenser as follows:

$$q = \rho_0 V_0(x) \left[h_0(x) + \frac{V_0^2(x)}{2} \right]. \tag{13}$$

In addition to the above boundary conditions, one needs to specify the initial conditions for the appropriate variables in the problem corresponding to the experimental conditions. This information is described in Section 5.

3. FRICTION COEFFICIENTS

The turbulence intensity in the simulated heat pipe was measured in ref. [11] to determine the characteristics of the vapor flow. For axial Reynolds numbers up to 10^6, laminar flow was observed in the blowing section and was retained in the suction section for axial Reynolds numbers less than 12000. The transition from laminar to fully turbulent was predicted in the entrance region of the suction section for axial Reynolds numbers greater than 12000. Unlike flow in impermeable tubes, laminar flow was maintained for axial Reynolds numbers greater than 2000. For the supersonic case in the suction and blowing section the flow remained laminar until a shock wave occurred and then turbulent flow abruptly appeared, which showed that no transition region existed.

Since the mathematical model is one-dimensional, proper expressions for the friction coefficient are necessary to take into account the frictional losses. Eleven numerical simulations were carried out in ref. [11] by using the two-dimensional numerical model to evaluate the friction coefficients according to the characteristics of the vapor flow. The following expressions for the friction coefficients including the compressibility effect were correlated by using the friction coefficients obtained from the two-dimensional

model. The friction coefficient for laminar flow in the condenser or the evaporator is

$$f = \frac{16}{Re}(1.2337 - 0.2337\,e^{-0.0363Re_0})\,e^{1.2M^2}. \quad (14)$$

The absolute value of the radial Reynolds number at the wall, Re_0, is used in the evaporator and the condenser. For the adiabatic section where the wall radial Reynolds number is zero, equation (14) is identical to that for the impermeable circular tube. For fully-developed turbulent flow in the condenser, the friction coefficient is

$$f_t = \frac{0.046}{Re^{0.2}}\left[1 + 55Re^{0.1}\left(\frac{V_0(x)}{U}\right)^{0.9}\left(\frac{2L_c}{D_v}\right)^{0.1} e^{1.2M^2}\right]. \quad (15)$$

For transition flow in the condenser entrance region, the friction coefficient is defined as

$$f = f_t + (f_c - f_t)\,e^{-0.412\bar{x}^2}. \quad (16)$$

For the one-dimensional numerical model presented in this paper, the vapor flow in the evaporator and adiabatic sections is assumed to be laminar. In the condenser, laminar flow is assumed for the axial Reynolds numbers below 12 000 at the entrance of the condenser and for supersonic flow. When the axial Reynolds number is greater than 12 000, transition and turbulent flows are considered in the condenser. Also, after a shock wave turbulent flow is assumed in the condenser. Equation (14) is used to evaluate the friction coefficients in the evaporator and adiabatic sections and is also employed in the condenser when the axial Reynolds number at the entrance of the condenser is less than 12 000 and the vapor flow is supersonic. When the axial Reynolds number is larger than 12 000, equation (16) is applied to the transition region, which is assumed to exist from the entrance of the condenser to about 60% of the condenser length, based on the experimental data shown in Fig. 3.8 in ref. [11]. Equation (15) is used for the turbulent flow in the condenser. The initial location of the transition region, $x_{t,i}$, is at the entrance of the condenser, and from Fig. 3.8 in ref. [11], $x_{t=3/4}$ and $x_{t=1/4}$ were estimated to be 0.7 and 0.6, respectively.

4. NUMERICAL FORMULATION

From the many schemes [16] available for the solution of the compressible flow problem, the Beam-Warming finite difference scheme is chosen to transform the governing equation (1) to the finite difference formulation. This scheme is a non-iterative implicit method and is similar to ADI for multidimensional flow problems by using the factorization which retains the tridiagonal block matrix.

The spatial derivatives are approximated by using the three-point second-order accurate central difference approximation for the interior points and the one-sided second-order accurate difference approximation for the boundary nodes. After the approximation operators are applied, the system of equations becomes

$$[J_{i-1}]\delta^n D_{i-1} + [K_i]\delta^n D_i + [L_{i+1}]\delta^n D_{i+1} = [\mathrm{RHS}]_i^n \quad i = 2, \ldots, I_{\max-1} \quad (17)$$

where

$$\delta^n D = D^{n+1} - D^n$$

$$[J_{i-1}] = -\frac{\theta_1 \delta t}{1+\theta_2}\left[\frac{1}{2\delta x}([A]^n - [P]^n + [R_v]^n) + \frac{1}{\delta x^2}[R]^n\right]_{i-1}$$

$$[K_i] = [I] - \frac{\theta_1 \delta t}{1+\theta_2}\left[[S]_i^n - \frac{2}{\delta x^2}[R]^n\right]$$

$$[L_{i+1}] = \frac{\theta_1 \delta t}{1+\theta_2}\left[\frac{1}{2\delta x}([A]^n - [P]^n + [R_v]^n) - \frac{1}{\delta x^2}[R]^n\right]$$

$$[\mathrm{RHS}]_i^n = \frac{\delta t}{1+\theta_2}\left[\frac{1}{2\delta x}(-E_{i+1}^n + E_{i-1}^n + F_{i+1}^n - F_{i-1}^n) + G_i^n\right] + \frac{\theta_2}{1+\theta_2}\delta^{n-1}D_i - \varepsilon(D_{i+2}^n - 4D_{i+1}^n + 6D_i^n - 4D_{i-1}^n + D_{i-2}^n)$$

where $[I]$ is the unit matrix, $[A]$, $[P]$, $[R]$ and $[S]$ are the Jacobian matrices, and ε the coefficient of the dissipative term to dampen oscillations.

This time difference formula reproduces many different schemes with the appropriate choice of θ_1 and θ_2. The scheme is second-order accurate in time when $\theta_1 = 1/2 + \theta_2$ and first-order accurate otherwise. For $\theta_1 = 1$ and $\theta_2 = 1/2$, the formula becomes second-order accurate in time over three grid points. The system of equations (17) has the following block tridiagonal structure:

$$[JKL]\{\delta^n D_i\} = \{\mathrm{RHS}_i^n\} \quad (18)$$

where $[JKL]$ represents the banded coefficient matrix of which components are 3×3 matrices for one-dimensional vapor flow, and $\{\delta^n D_i\}$ and $\{\mathrm{RHS}_i^n\}$ are column vectors. The tridiagonal block matrix size is now $(3 \times I_{\max-2}) \times (3 \times I_{\max-2})$ where $I_{\max}$ is the number of nodal points. This system of equations can be solved using the conventional methods for solving block tridiagonal systems of equations. The vector of unknowns at the $n+1$th time step is then determined by simply adding $\delta^n D$ to the value of D^n at the nth step. The primitive variables (ρ, U, P, T) can be obtained from D^{n+1}.

A total of 80 nodes, which is the minimum number of nodes to obtain accurate results, are evenly spaced in the axial direction and a time step of 0.1×10^{-3} s is

used for the simulated heat pipe vapor flow. Since the heat flux at the wall in the evaporator is different from that in the condenser due to the different lengths for the cylindrical heat pipe, the coarse nodal system presented some difficulty in reaching the steady state. For the cylindrical heat pipe, 200 evenly-spaced nodes are used in the axial direction and a time step of 0.1×10^{-3} s is employed.

5. RESULTS AND DISCUSSION

5.1. *Comparison with the simulated heat pipe vapor flow*

A comparison of the numerical results with the experimental data given in ref. [11] is desired to verify the mathematical model and algorithm. However, the existing experimental data was obtained by simulating the vapor flow of a cylindrical heat pipe with a porous pipe which has an inside diameter of 1.65 cm and a length of 0.61 m as shown in Fig. 1. The blowing and suction sections have equal lengths and were simulated by the injection and suction of air without phase change at the interface. Also, uniform source and sink pressures for the blowing and suction regions are specified instead of the radial mass flow rate. Thus, to simulate the experiment equation (12) is used to obtain the radial mass flux with the known source and sink pressures.

5.1.1. *Transient results.* The existing experimental data were obtained at the steady state so the present transient numerical results can only be compared with the transient numerical results for the two-dimensional model [11]. For this purpose, the same geometry and physical conditions are used such as the source pressure of 2.06×10^5 N m^{-2} (30 psia) and the sink pressure of 1.03×10^5 N m^{-2} (15 psia) corresponding to case B.1.

Initially, the velocity of the vapor is zero and the pressure and temperature are the same as the source pressure and temperature, respectively. To simulate the transient flow, the sink pressure is suddenly lowered to 1.03×10^5 N m^{-2} (15 psia), while the source pressure remains the same as the initial pressure. This difference between the source and sink pressures initiates the air flow from the blowing section to the suction section. The pressures at the inlet of the blowing section, the center of the pipe, and the end of the suction section are plotted to compare with the numerical results for the two-dimensional model as shown in Fig. 2.

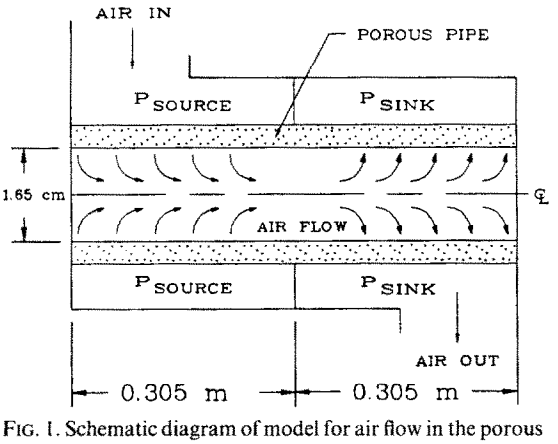

FIG. 1. Schematic diagram of model for air flow in the porous pipe.

Figure 2 shows the following transient behavior of the air flow in the porous pipe. Since the sink pressure is abruptly changed from the initial pressure to 1.03×10^5 N m^{-2} (15 psia) along the entire suction section, the pressures at the center and last nodes decrease immediately due to the evacuation of air. For this period, the blowing section pressures adjacent to the suction section start to decrease due to the flow of mass from the blowing section to the suction section, but the pressure near the beginning of the blowing section remains constant. Also, the mass flow rate from the blowing section to the suction section is not sufficient to influence the end of the suction section so that the pressure at this point decreases faster than that at the center of the pipe.

At about 0.8×10^{-3} s, the pressure at the end of the suction section reaches the minimum value and then starts to increase while the pressure at the center of the pipe keeps decreasing due to the frictional loss and the acceleration of the flow. At this time, the pressures over the entire blowing section become less than the initial pressure so that the mass flow rate is sufficient to influence the end of the suction section. As the pressure in the blowing section decreases and the source pressure remains constant, the mass flow rate from the blowing section to the suction section increases. Thus, the pressure at the center node keeps decreasing and the pressure at the end of the suction section rises due to the contribution of the mass from the blowing section.

At about 3.5×10^{-3} s, the pressures at all three points reach the steady state. As expected, the pressure at the end of the suction section does not recover completely due to the frictional loss at the pipe wall. Figure 2 shows that the present results and numerical results for the two-dimensional model [11] are in agreement.

5.1.2. *Steady state results.* When the present numerical results reach the steady state, those results are compared with the experimental data given in ref. [11]. Numerical calculations are conducted for four different sets (i.e. cases B.2, B.3, B.4, and B.5) of the source and sink pressures by using equations (14)–(16) for the friction coefficient. The cases examined are as follows:

Case B.2: $P_{so} = 1.39 \times 10^5$ and $P_{sk} = 1.21 \times 10^5$ N m^{-2}

Case B.3: $P_{so} = 2.09 \times 10^5$ and $P_{sk} = 1.57 \times 10^5$ N m^{-2}

Case B.4: $P_{so} = 2.68 \times 10^5$ and $P_{sk} = 1.69 \times 10^5$ N m^{-2}

Case B.5: $P_{so} = 5.30 \times 10^5$ and $P_{sk} = 1.06 \times 10^5$ N m^{-2}.

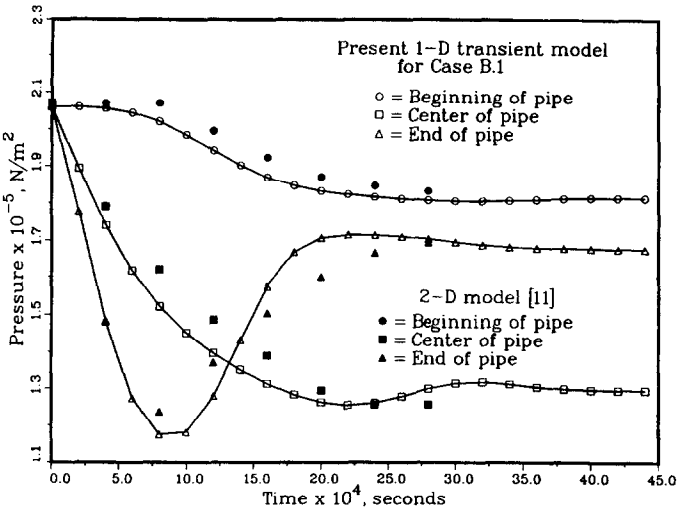

FIG. 2. Comparison of the present numerical results with Bowman's two-dimensional model for pressure variations with time at three locations of the porous pipe: case B.1.

Figure 3 shows the comparison of the pressure distributions along the axial direction. The top three lines in Fig. 3 show the pressure distributions for the low mass flow rates. The pressures in the blowing section decrease due to friction and the acceleration of the flow caused by mass injection, but the pressures in the suction section increase owing to the deceleration of the flow by the extraction of mass. However, the pressures at the end of the suction section are less than those at the beginning of the blowing section because of the loss due to friction. In these three cases, the pressure distributions at the steady state correspond well to those for low temperature heat pipes and are in agreement with the experimental data.

The fourth data profile (case B.5) shows the pressure variation in the axial direction for the high mass flow rate. Unlike the previous three cases, the pressure drop in the blowing section is very large. The pressure ratio at the exit of the blowing section is about 0.4 and this ratio corresponds to a Mach number of $M = 1$. After the pressure decreases in the blowing section, the pressure keeps decreasing in the entrance region of the suction section due to the expansion of air even though mass removal occurs. Then, the pressure suddenly increases and then continues to increase as the flow slows down. This implies that a shock wave occurs at the place where the pressure changes abruptly. When a shock wave does not exist in the suction section, the pressure is supposed to decrease along the suction section. The one-dimensional model predicts the supersonic flow and shock wave in the suction section and the comparison of the numerical results and experimental data shows a good agreement except for the region immediately after the shock wave.

The variations of the pressure and velocity at the

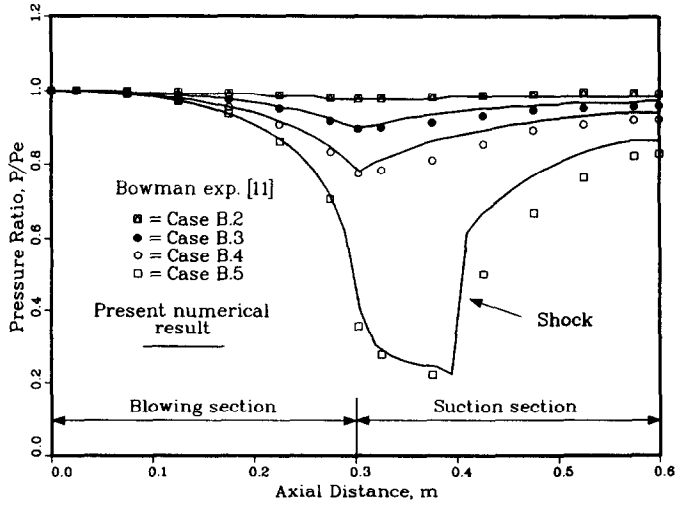

FIG. 3. Comparison of the present numerical results with the experimental pressure variations [11] in the porous pipe.

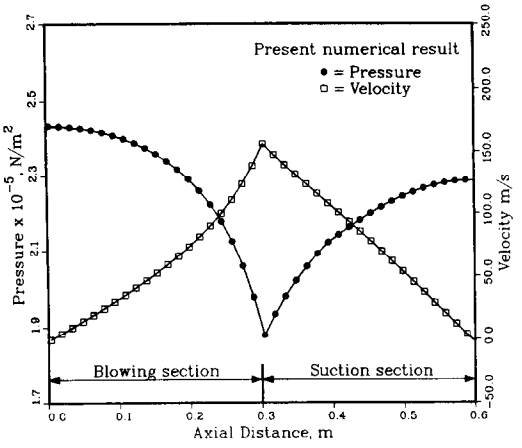

FIG. 4. Axial variations of pressure and velocity for case B.4.

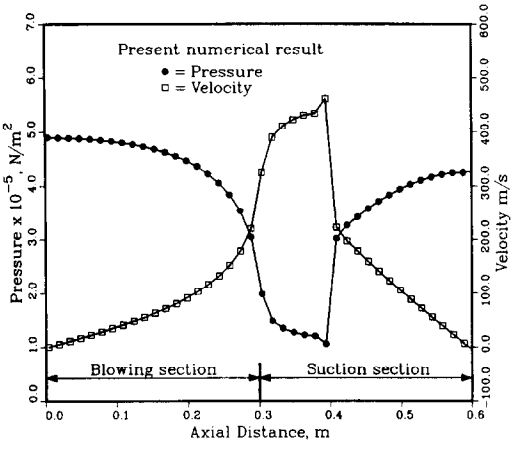

FIG. 5. Axial variations of pressure and velocity for case B.5.

steady state corresponding to cases B.4 and B.5 are shown in Figs. 4 and 5, respectively. For the low mass flow rate, the temperature and density in the blowing section decrease corresponding to the decrease in pressure and the velocity increases due to the mass injection. The Mach number, M, however, is less than 1 at the exit of the blowing section, so the velocity in the suction section decreases because of the extraction of mass. Also, the temperature and density should increase in the suction section. Figure 5 shows the axial variations of the pressure and velocity for the high mass flow rate. After the sonic velocity is reached at the exit of the blowing section, the velocity keeps increasing in the suction section until a shock wave occurs. Then, the velocity decreases to zero at the end of the pipe. The air expands near the entrance region of the suction section and then the density suddenly increases after the shock wave.

5.2. *Comparison with actual vapor flow in cylindrical heat pipes*

The model was tested for the actual vapor flow in a sodium heat pipe corresponding to the experiment

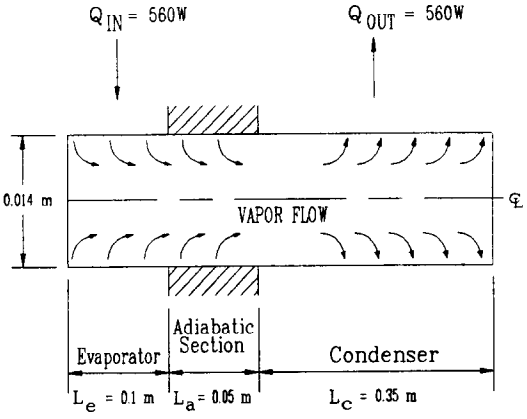

FIG. 6. Schematic diagram of model for the sodium vapor flow in the heat pipe.

given in ref. [15] as shown in Fig. 6. The lengths of the evaporator, adiabatic, and condenser sections are 0.1, 0.05, and 0.35 m, respectively. The diameter of the vapor space is 0.014 m. The experimental data [15] represents only the saturation temperature and heat transfer rate (Q = 560 W) at the steady state. The initial conditions and actual boundary conditions applied on the surface of the evaporator and condenser are unknown. The present numerical model is transient, however, so the initial conditions and history of heat input and output in the evaporator and condenser sections are needed.

For the numerical calculations, the uniform initial temperature of 810 K is used and the vapor is assumed to be saturated at the initial temperature. Initially, the velocity of the vapor is zero. The same amount of heat (Q = 560 W) is uniformly applied on the surface of the evaporator and the convective boundary condition is used on the surface of the condenser. The reference temperature of 300 K for the convective boundary condition is employed and the heat transfer coefficient is determined by iteration. At first, an arbitrary initial heat transfer coefficient is guessed. When the numerical results reach the steady state, the saturation temperature at the end cap of the evaporator is compared with the experimental data at the same location. This procedure is repeated until the same temperature is obtained at the steady state. For this test, the heat transfer coefficient of 69.1 W m^{-2} K^{-1} is used.

Figure 7 shows the axial variation of the saturation and vapor temperatures, pressure, velocity and density obtained from the present numerical model and the experimentally measured saturation temperature distribution [15]. The pressure, temperature and density in the evaporator decrease and the velocity increases due to the injection of mass and the effect of friction. In the adiabatic section, the pressure decreases owing to friction at the interface. The density also decreases while the velocity continues to increase. The pressure recovery in the condenser is almost negligible. This is due to the dominant friction

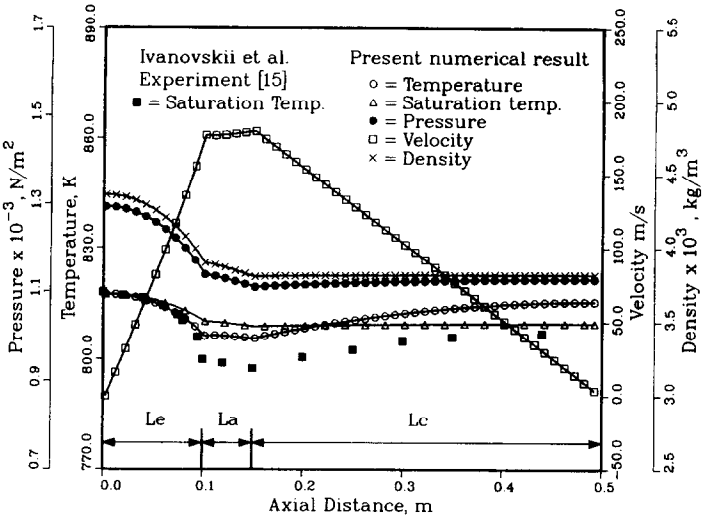

FIG. 7. Axial variations of temperature, pressure, velocity and density of the sodium heat pipe at steady state.

effect at the interface of the condenser compared to the effect of mass extraction in this long condenser. In the adiabatic section a difference between the calculated and measured saturation temperatures is observed, but the trend of the saturation temperature variation is the same. The trend of the vapor temperature in the condenser is quite different from that of the saturation temperature in the same region, so the saturation temperature may not be assumed to be the vapor temperature in the condenser for the one-dimensional model. It should be noted that the effects of the wall and the wick should be included in the transient analysis of actual heat pipes.

6. CONCLUSIONS

A model for the transient one-dimensional compressible vapor flow in the cylindrical heat pipe is developed. This model predicts the vapor flow in cylindrical heat pipes as well as simulated heat pipes for the subsonic, sonic, and supersonic flows under transient and steady state conditions. For the simulated heat pipe, the vapor flow quickly reaches the steady state condition. The distributions of the temperature and pressure during the transient state are quite different from those for the steady state. The one-dimensional compressible model predicts the experimental data well for the cylindrical heat pipe and the simulated heat pipe at the steady state. The experimental data for the transient state are needed to understand clearly the transient behavior of the vapor flow in the heat pipe both at low and high temperatures. The one-dimensional model can reduce the computational effort needed to solve the vapor flow problem.

Acknowledgement—Funding for this work was provided by a joint effort of the NASA Lewis Research Center and the Thermal Energy Group of the Aero Propulsion and Power Laboratory of the U.S. Air Force under contract F33615-88-C-2820.

REFERENCES

1. E. K. Levy, Theoretical investigation of heat pipes operating at low vapor pressures, *J. Engng Ind.* **90,** 547–552 (1968).
2. Y. M. Brovalsky, P. I. Bystrov and M. V. Melkinov, The method of calculation and investigation of high-temperature heat pipe characteristics taking into account the vapor flow compressibility, friction, and velocity profile, *Proc. 2nd Int. Heat Pipe Conf.*, pp. 113–122 (1976).
3. A. Faghri, Performance characteristics of a concentric annular heat pipe—part II. Vapor flow analysis, *ASME J. Heat Transfer* **111**(4), 851–857 (1989).
4. J. H. Jang, An analysis of startup from the frozen state and transient performance of heat pipes, Ph.D. Dissertation, Georgia Institute of Technology (1988).
5. C. A. Bankston and H. J. Smith, Incompressible laminar vapor flow in cylindrical heat pipes, ASME Paper No. 71-WA/HT-15 (1972).
6. C. L. Tien and A. R. Rohani, Analysis of the effects of vapor pressure drop on heat pipe performance, *Int. J. Heat Mass Transfer* **17,** 61–67 (1974).
7. H. V. Ooijen and C. J. Hoogendoorn, Vapor flow calculations in flat-plate heat pipe, *AIAA J.* **17**(11), 1251–1259 (1979).
8. A. Faghri, Vapor flow analysis in a double-walled concentric heat pipe, *Numer. Heat Transfer* **10**(6), 583–595 (1986).
9. M. M. Chen and A. Faghri, An analysis of the vapor flow and the heat conduction through the liquid-wick and pipe wall in a heat pipe with single or multiple heat sources, *Int. J. Heat Mass Transfer* **33,** 1945–1955 (1990).
10. Y. Cao, A. Faghri and E. T. Mahefkey, The thermal performance of heat pipes with localized heat input, *Int. J. Heat Mass Transfer* **32,** 1279–1287 (1989).
11. W. J. Bowman, Simulated heat pipe vapor dynamics, Ph.D. Dissertation, Air Force Institute of Technology (1987).
12. W. J. Bowman and J. Hitchcock, Transient, compressible heat-pipe vapor dynamics, *Proc. 25th ASME Natn. Heat Transfer Conf.*, Houston, Texas, pp. 329–337 (1988).
13. Y. Cao and A. Faghri, Transient two-dimensional compressible analysis for high-temperature heat pipes with

pulsed heat input, *Numer. Heat Transfer* **18**, 483–502 (1990).
14. J. H. Jang, A. Faghri, W. S. Chang and E. T. Mahefkey, Mathematical modeling and analysis of heat pipe start-up from frozen state, *ASME J. Heat Transfer* **112**(3), 586–594 (1990).
15. M. N. Ivanovskii, V. P. Sorokin and I. V. Yagodkin, *The Physical Principles of Heat Pipes*. Clarendon Press, Oxford (1982).
16. D. A. Anderson, J. C. Tannehill and R. H. Pletcher, *Computational Fluid Mechanics and Heat Transfer*. Hemisphere, New York (1984).

ANALYSE DU TRANSPORT MONODIMENSIONNEL VARIABLE DE VAPEUR COMPRESSIBLE DANS LES CALODUCS

Résumé—On modélise l'écoulement variable monodimensionnel de vapeur dans un caloduc. Les résultats numériques sont obtenus en utilisant la méthode implicite non itérative aux différences finies Beam-Warming. Le modèle est testé pour l'écoulement de vapeur simulé et celui réel dans des caloducs cylindriques. On obtient une bonne comparaison des résultats pour l'écoulement simulé de vapeur et pour les résultats transitoires antérieurs d'un modèle bidimensionnel et les résultats de régime permanent sont en accord avec les données expérimentales existantes. Le comportement variable de l'écoulement de vapeur aux vitesses subsonique, sonique et supersonique aussi bien que les débits masse élevés sont prédits avec succès.

ANALYTISCHE UNTERSUCHUNG DER EINDIMENSIONALEN TRANSIENTEN KOMPRESSIBLEN DAMPFSTRÖMUNG IN WÄRMEROHREN

Zusammenfassung—Das dynamische Verhalten einer kompressiblen eindimensionalen Dampfströmung in einem Wärmerohr wird modellhaft dargestellt. Mit Hilfe der impliziten nicht-iterativen "BEAM-WARMING"-Finite-Differenzen-Methode werden numerische Ergebnisse ermittelt. Das Modell wird für simulierte Dampfströmungen in einem Wärmerohr und für tatsächliche Dampfströmungen in zylindrischen Wärmerohren überprüft. Das transiente Verhalten der simulierten Dampfströmung in einem Wärmerohr stimmt gut mit früheren Ergebnissen aufgrund eines zweidimensionalen numerischen Modells überein; die stationären Ergebnisse stimmen mit vorhandenen Versuchsdaten überein. Das transiente Verhalten der Dampfströmung bei Unterschall-, Schall- und Überschallgeschwindigkeit wie auch bei hohen Massenstromdichten wird erfolgreich vorhergesagt.

АНАЛИЗ ОДНОМЕРНОГО НЕСТАЦИОНАРНОГО ТЕЧЕНИЯ СЖИМАЕМОГО ПАРА В ТЕПЛОВЫХ ТРУБАХ

Аннотация—Моделируется динамика нестационарного одномерного течения сжимаемого пара в тепловой трубе. Численные результаты получены с использованием неявного неитерационного конечно-разностного метода Бима-Уорминга. Найденные результаты сопоставляются с данными по реальному течению пара в цилиндрических тепловых трубах. Достигнуто хорошее согласие между нестационарными результатами, полученными для модельного течения пара в тепловой трубе, и прежними результатами по двумерной численной модели, а также между стационарными результатами и имеющимися экспериментальными данными. Успешно предсказывается нестационарное поведение течения пара при дозвуковых, звуковых и сверхзвуковых скоростях, а также высокие значения массового расхода пара.